Available online at www.sciencedirect.com
SCIENCE DIRECT®
Applied Mathematical Modelling 30 (2006) 702–713
APPLIED MATHEMATICAL MODELLING
www.elsevier.com/locate/apm

Algebraic Dirichlet-to-Neumann mapping for linear elasticity problems with extreme contrasts in the coefficients

Frédéric Magoulès [a,*], François-Xavier Roux [b], Laurent Series [b]

[a] Institut Elie Cartan de Nancy, Université Henri Poincaré, BP 239, 54506 Vandoeuvre-les-Nancy Cedex, France
[b] High Performance Computing Unit, ONERA, 29 av. de la Division Leclerc, BP 72, 92322 Châtillon Cedex, France

Received 10 June 2005; received in revised form 28 June 2005; accepted 5 July 2005
Available online 22 December 2005

Abstract

The convergence of iterative based domain decomposition methods is linked with the absorbing boundary conditions defined on the interface between the sub-domains. For linear elasticity problems, the optimal absorbing boundary conditions are associated with non-local Dirichlet-to-Neumann maps. Most of the methods to approximate these non-local maps are based on a continuous analysis. In this paper, an original algebraic technique based on the computation of local Dirichlet-to-Neumann maps is investigated. Numerical experiments are presented for linear elasticity problems with extreme contrasts in the coefficients.

Keywords: Dirichlet-to-Neumann; Domain decomposition; Discontinuous coefficients; Heterogeneous media; Linear elasticity

1. Introduction

Domain decomposition methods with Lagrange multipliers have been shown to be very efficient for the parallel solution of large scale problems [1–4]. These methods are based on the partitioning of the global domain into non-overlapping sub-domains. The continuity is enforced by using additional (one or two) Lagrange multipliers [5] across the interfaces between the sub-domains. Additional augmented matrices defined on the interface are used in order to avoid possible non-well-posed sub-problems [6–8]. The definition of theses augmented matrices is linked with the absorbing boundary conditions defined on the interface between the sub-domains [9,10]. It can be shown that using some absorbing boundary conditions involving a non-local Dirichlet-to-Neumann (DtN) map of the outside of each sub-domain, leads to the optimal convergence of the iterative domain decomposition algorithm based on two Lagrange multipliers [11,12]. Several approaches have been investigated to define efficient local approximation of this DtN map. These approximations can be classified

* Corresponding author. Tel.: +33 383 684564; fax: +33 3 83 684534.
E-mail addresses: frederic.magoules@iecn.u-nancy.fr (F. Magoulès), francois-xavier.roux@onera.fr (F.-X. Roux), laurent.series@onera.fr (L. Series).

0307-904X/$ - see front matter © 2005 Elsevier Inc. All rights reserved.
doi:10.1016/j.apm.2005.07.008

into two major classes. The first class consists of continuous approximations of the continuous DtN operator with Fourier analysis tools [13–17]. The second class consists of discrete approximations of the discrete DtN operator with algebraic techniques [18,12,19]. In this paper, an original technique is introduced. This technique consists to define several local DtN maps and to assembly these local DtN maps in order obtain an efficient and robust approximation of the non-local DtN map.

This paper is organized as follows: Section 2 introduces the equations of linear elasticity and the linear system of equations considered. Section 3 presents the domain decomposition method with two Lagrange multipliers and two augmented matrices defined on the interface between the sub-domains. The non-local Dirichlet-to-Neumann map involved for the optimal convergence of this domain decomposition method is then briefly reminded. Section 4 introduces an original technique to approximate this non-local Dirichlet-to-Neumann map. The analogy of this original technique with a finite element method is then discussed. An asymptotic analysis of this technique is presented in Section 5, followed by numerical experiments applied to linear elasticity problems with extreme contrasts in the coefficients. Finally, Section 6 contains the conclusions of this paper.

2. Mathematical formulation

Here, the equations of linear elasticity are considered. Let an elastic body which occupies in the absence of force the set $\Omega \in \mathbb{R}^3$ with a regular boundary $\partial\Omega$. Let $u_i(x,t)$ denotes the displacement at position x ($x \in \mathbb{R}^3$). The symmetric strain tensor (Green tensor) ϵ_{ij} is defined by

$$\epsilon_{ij} = \frac{1}{2}(\partial_{x_j} u_i + \partial_{x_i} u_j + \partial_{x_i} u_k \partial_{x_j} u_k).$$

Assuming small displacements $\partial_{x_i} u_j \ll 1$ and small strain $\partial_{x_i} u_i \ll 1$, the linear expression of the strain tensor reduces to

$$\epsilon_{ij} = \frac{1}{2}(\partial_{x_j} u_i + \partial_{x_i} u_j).$$

In the case of an hyper-elastic body, the strain and stress tensor are linked together with the relationship:

$$\sigma_{ij} = g(\epsilon_{kl}).$$

In the following analysis, the case of a linear body is considered which means that the stress tensor is proportional to the strain tensor:

$$\sigma_{ij} = C_{ijkl}\ \epsilon_{kl}.$$

Finally, in the case of an isotropic body the Hooke law gives

$$\sigma_{ij} = \lambda\ \epsilon_{kk}\delta_{ij} + 2\mu\ \epsilon_{ij},$$

where

$$\lambda = \frac{Ev}{(1+v)(1-2v)} \text{ and } \mu = \frac{E}{2(1+v)},$$

denote the Lamé coefficients, E the Young modulus and v the Poisson ratio. With these notations, applying the Hamilton principle to the continuous system of equations and assuming small displacements, the system of equations of linear elasticity can be obtained:

$$-(\lambda+\mu)\nabla(\mathrm{div}(u)) - \mu\Delta u = f, \tag{2.1}$$

where f denotes the right-hand side. The variational formulation of this system of equations gives find $u \in H^1(\Omega)$ such as $\forall v \in H^1(\Omega)$

$$a(u,v) = l(v),$$

where

$$a(u,v) = \int_\Omega \left(\lambda \text{ div } u(x) \text{ div } v(x) + 2\mu \sum_{i,j=1}^{3} \epsilon_{ij}(u(x))\epsilon_{ij}(v(x)) \right) \mathrm{d}x,$$

$$l(v) = \int_\Omega f(x)\ v(x)\, \mathrm{d}x.$$

The ellipticity of the bilinear form and the well-posedness of the linear system (2.1) can be obtained through the Korn inequalities [20].

3. Iterative domain decomposition method

3.1. Introducing Lagrange multipliers and augmented matrices

The global domain Ω is meshed and partitioned into two sub-domains $\Omega^{(1)}$ and $\Omega^{(2)}$ without overlap and with an interface $\Gamma = \Omega^{(1)} \cap \Omega^{(2)}$. Let $K^{(s)}$, and $b^{(s)}$ denote, respectively, the stiffness matrix, and the right-hand side vector associated with the sub-domain $\Omega^{(s)}$, and let $u^{(s)}$ denotes the restriction to $\Omega^{(s)}$ of the solution of the global problem. Let denote by the subscripts i and p the internal and interface boundary unknowns, respectively. With these notations the local stiffness matrix, the local solution and the right-hand side can be written:

$$K^{(s)} = \begin{pmatrix} K_{ii}^{(s)} & K_{ip}^{(s)} \\ K_{pi}^{(s)} & K_{pp}^{(s)} \end{pmatrix}, \quad u^{(s)} = \begin{pmatrix} u_i^{(s)} \\ u_p^{(s)} \end{pmatrix}, \quad b^{(s)} = \begin{pmatrix} b_i^{(s)} \\ b_p^{(s)} \end{pmatrix}.$$

The global problem is a block system obtained by assembling local contribution of each sub-domain:

$$\begin{pmatrix} K_{ii}^{(1)} & 0 & K_{ip}^{(1)} \\ 0 & K_{ii}^{(2)} & K_{ip}^{(2)} \\ K_{pi}^{(1)} & K_{pi}^{(2)} & K_{pp} \end{pmatrix} \begin{pmatrix} u_i^{(1)} \\ u_i^{(2)} \\ u_p \end{pmatrix} = \begin{pmatrix} b_i^{(1)} \\ b_i^{(2)} \\ b_p \end{pmatrix}, \tag{3.1}$$

where $K_{pp} = K_{pp}^{(1)} + K_{pp}^{(2)}$ and where $b_p = b_p^{(1)} + b_p^{(2)}$.

From the previous partition, it is clear [7,12] that the global problem is equivalent to the local sub-problems

$$\begin{pmatrix} K_{ii}^{(1)} & K_{ip}^{(1)} \\ K_{pi}^{(1)} & K_{pp}^{(1)} + A_{pp}^{(1)} \end{pmatrix} \begin{pmatrix} u_i^{(1)} \\ u_p^{(1)} \end{pmatrix} = \begin{pmatrix} b_i^{(1)} \\ b_p^{(1)} + \lambda^{(1)} \end{pmatrix}, \tag{3.2}$$

$$\begin{pmatrix} K_{ii}^{(2)} & K_{ip}^{(2)} \\ K_{pi}^{(2)} & K_{pp}^{(2)} + A_{pp}^{(2)} \end{pmatrix} \begin{pmatrix} u_i^{(2)} \\ u_p^{(2)} \end{pmatrix} = \begin{pmatrix} b_i^{(2)} \\ b_p^{(2)} + \lambda^{(2)} \end{pmatrix}, \tag{3.3}$$

under both the admissibility constraint

$$u_p^{(1)} = u_p^{(2)}, \tag{3.4}$$

and the modified equilibrium constraint

$$A_{pp}^{(1)} u_p^{(1)} + A_{pp}^{(2)} u_p^{(2)} = \lambda^{(1)} + \lambda^{(2)}, \tag{3.5}$$

where $A_{pp}^{(s)}$ is an augmented matrix defined on the interface and where $\lambda^{(s)}$ is a Lagrange multiplier, for $s = 1, 2$. Eqs. (3.2) and (3.3) can be interpreted as the discretization of two sub-domain linear elasticity sub-problems with the following absorbing boundary conditions on the interface:

$$\sigma^{(1)}(u^{(1)}) \cdot n^{(1)} + \mathscr{A}^{(1)} u^{(1)} = \lambda^{(1)} \quad \text{on } \Gamma, \tag{3.6}$$

$$\sigma^{(2)}(u^{(2)}) \cdot n^{(2)} + \mathscr{A}^{(2)} u^{(2)} = \lambda^{(2)} \quad \text{on } \Gamma, \tag{3.7}$$

where $\mathscr{A}^{(s)}$ is the continuous operator associated to the matrix $A_{pp}^{(s)}$, and $n^{(s)}$ is the outward normal unitary vector of the sub-domain $\Omega^{(s)}$ along the interface Γ. It is well known that during the domain partitioning,

non-well-posed linear elasticity sub-problems may appear [2]. In this case, an additional procedure for the detection of the rigid body motions of the sub-domains is mandatory [5]. The purpose of a carefully constructed matrix $A_{pp}^{(s)}$ is to prevent the singularity of the sub-domain matrix. In other words, the detection of the rigid body motions is no longer required to solve the linear elasticity sub-problems, even in the case of general domain partitioning.

A combination of Eqs. (3.4) and (3.5), leads to the following continuity constraints:

$$\lambda^{(1)} + \lambda^{(2)} - A_{pp}^{(1)} u_p^{(2)} - A_{pp}^{(2)} u_p^{(2)} = 0, \tag{3.8}$$

$$\lambda^{(1)} + \lambda^{(2)} - A_{pp}^{(1)} u_p^{(1)} - A_{pp}^{(2)} u_p^{(1)} = 0. \tag{3.9}$$

The variables $u_i^{(1)}$ and $u_i^{(2)}$ can be eliminated from Eqs. (3.2) and (3.3) in favor of $u_p^{(1)}$ and $u_p^{(2)}$, which gives after substitution in Eqs. (3.8) and (3.9), the following linear system:

$$F\lambda = d, \tag{3.10}$$

where the matrix F, the vector λ and the right-hand side d are

$$F = \begin{pmatrix} I & I - (A_{pp}^{(1)} + A_{pp}^{(2)})[S_{pp}^{(2)} + A_{pp}^{(2)}]^{-1} \\ I - (A_{pp}^{(1)} + A_{pp}^{(2)})[S_{pp}^{(1)} + A_{pp}^{(1)}]^{-1} & I \end{pmatrix},$$

$$\lambda = \begin{pmatrix} \lambda^{(1)} \\ \lambda^{(2)} \end{pmatrix}, \quad d = \begin{pmatrix} (A_{pp}^{(1)} + A_{pp}^{(2)})[S_{pp}^{(2)} + A_{pp}^{(2)}]^{-1} c_p^{(1)} \\ (A_{pp}^{(1)} + A_{pp}^{(2)})[S_{pp}^{(1)} + A_{pp}^{(1)}]^{-1} c_p^{(2)} \end{pmatrix},$$

with $S_{pp}^{(s)} = K_{pp}^{(s)} - K_{pi}^{(s)}[K_{ii}^{(s)}]^{-1} K_{ip}^{(s)}$ the Schur complement matrix and $c_p^{(s)}$ the condensed right-hand side in the sub-domain $\Omega^{(s)}$.

3.2. Non-local Dirichlet-to-Neumann maps

An iterative method is commonly used to solve the linear system (3.10). It can be proved that choosing each augmented matrix $A_{pp}^{(s)}$ equal to the complete outer Schur complement of each sub-domain, leads to the optimal convergence of the domain decomposition algorithm [18,12]. In the continuous analysis, this optimal selection consists of choosing as the operator $\mathscr{A}^{(s)}$ involved in the absorbing boundary conditions (3.6) and (3.7) a Steklov–Poincaré operator [11,21]. The Steklov–Poincaré operator and the complete outer Schur complement matrix are the continuous and the discrete expression of the Dirichlet-to-Neumann map of the outside of the sub-domain on its interface boundary. This non-local Dirichlet-to-Neumann map models the physical phenomena involved outside each domain $\Omega^{(s)}$.

Several approximations of this non-local operator have been performed, and can be classified into two major classes. The first class consists of continuous approximations of the continuous DtN operator with Fourier analysis tools [6,15,7,22], which are then discretized. In the particular case of extreme contrasts in the coefficients, the previous analysis is not straightforward and is still under current investigation. The second class consists of discrete approximations of the discrete non-local Dirichlet-to-Neumann operator with algebraic techniques [18,12,19]. The proposed techniques are based on SParse Approximate Inverse (SPAI) or on small non-local Dirichlet-to-Neumann maps. In this paper, an original technique based on the construction of several local Dirichlet-to-Neumann maps is investigated.

4. Local Dirichlet-to-Neumann maps

4.1. Motivation

The optimal choice of the absorbing boundary conditions (3.6) and (3.7) is linked with the DtN maps of the outside of each sub-domain. After a finite element discretization, this optimal choice leads to a dense augmented matrix $A_{pp}^{(s)}$ equal to the complete outer Schur complement matrix.

The exact computation of this outer Schur complement matrix requires a lot of operations and a lot of exchange of data between the sub-domains. To reduce this number of operations, a first approximation of the complete outer Schur complement by the Schur complement of the neighboring sub-domain only can be considered [18,12]. This approach consists to define a DtN map of the neighboring sub-domain on the interface. Despite the fact that the neighbor Schur complement matrix is a dense matrix, the computational cost and the exchange of data are reduced to the neighboring sub-domains only. This reduces significantly the CPU time.

Unfortunately, using the previous approximation (which is a dense matrix) as the augmented matrix $A_{pp}^{(s)}$ increases the bandwidth of the sub-domain matrix. This implies a lot of additional operations during the factorization of the sub-domain matrix and during the forward–backward substitutions required to solve the condensed interface problem. To reduce these costs, a sparse approximation can be considered. The technique proposed in the following sub-sections presents the advantage to keep the sparsity of the sub-domain matrix after the addition of the augmented matrix.

4.2. Mesh partitioning without cross points

The condensation procedure involved in the computation of the neighbor Schur complement represents the interactions of all the nodes inside the neighboring sub-domain and on the interface. In order to keep the sparsity of the augmented matrix, it may be interesting to limit these interactions only to part of the neighboring sub-domain. The approximation considered in this sub-section consists of the condensation of some degree of freedom inside the sub-domain on a small part of the interface, called patch. In order to describe this original approach, the case of a general domain Ω split into two non-overlapping sub-domains $\Omega^{(1)}$ and $\Omega^{(2)}$, with an interface Γ is now considered. The following subsets of indexes are defined for the nodes of the sub-domain $\Omega^{(s)}$, $s = 1, 2$:

$$
\begin{aligned}
V &= \{\text{indexes of nodes inside the sub} - \text{domain and on the interface}\},\\
V_\Gamma &= \{\text{indexes of nodes on the interface } \Gamma\},\\
V_r^{\{j\}} &= \text{indexes of nodes belonging to } V_\Gamma \text{ such that the minimum connectivity distance between}\\
&\qquad \text{each of these nodes and the node number } \{j\} \text{ is lower than } r, \quad r \in \mathbb{N},\\
V_{r,d}^{\{j\}} &= \text{indexes of nodes belonging to } V \text{ such that the minimum connectivity distance between}\\
&\qquad \text{each of these nodes and the nodes belonging to } V_r^{\{j\}} \text{ is lower than } d, \quad d \in \mathbb{N}.
\end{aligned}
$$

In other words, the subset $V_r^{\{j\}}$ corresponds to a patch of radius r around the node number $\{j\}$, and the subset $V_{r,d}^{\{j\}}$ corresponds to neighboring layers of depth d of the patch.

For the sake of clarity, an example is now detailed. For this purpose, a regular $\mathbb{P}_1$-finite element mesh of the domain Ω is considered with triangles, and this mesh is partitioned into two sub-domains with one interface. Fig. 1 represents the mesh partitioning. An example of the subset of indexes is shown in Fig. 3 for a numbering of the nodes illustrated in Fig. 2.

In order to build the approximation of the neighbor Schur complement matrix $K_{pp}^{(2)} - K_{pi}^{(2)}[K_{ii}^{(2)}]^{-1}K_{ip}^{(2)}$, this matrix is approximated with the matrix $A_{pp}^{(1)}$.

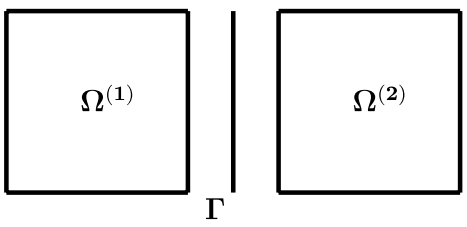

Fig. 1. Domain decomposition into two sub-domains.

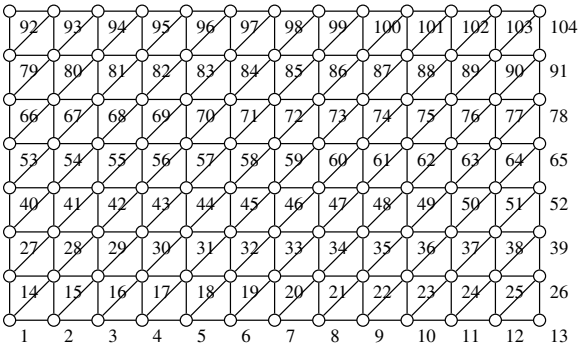

Fig. 2. Nodes number of the sub-domain $\Omega^{(2)}$.

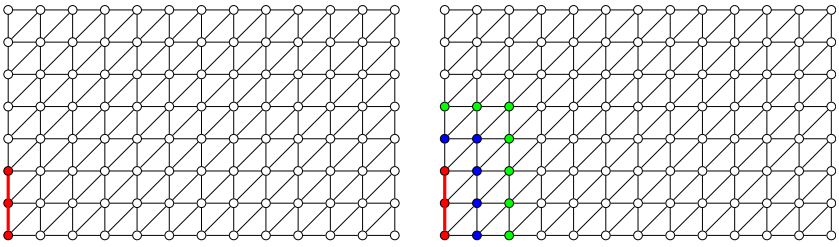

Fig. 3. Nodes of the sub-domain $\Omega^{(2)}$. On the left, the patch associated to the interface node number $\{14\}$ with a radius one, and on the right this patch and a depth equal to two. $V_1^{\{14\}} = \{1, 14, 27\}$, $V_{1,1}^{\{14\}} = V_1^{\{14\}} \cup \{2, 15, 28, 40, 41\}$, and $V_{1,2}^{\{14\}} = V_{1,1}^{\{14\}} \cup \{3, 16, 29, 42, 53, 54, 55\}$.

Algorithm 4.1. The complete algorithm to build the approximation of the neighbor Schur complement matrix $K_{pp}^{(2)} - K_{pi}^{(2)}[K_{ii}^{(2)}]^{-1}K_{ip}^{(2)}$ is defined as the following steps:

(1) Initialization of the radius r, and of the depth d.
(2) Construction of the sparse structure of the interface matrix $A_{pp}^{(1)} \in \mathbb{R}^{\dim V_\Gamma \times \dim V_\Gamma}$.
(3) Construction of the sparse structure of the sub-domain matrix $K^{(2)} \in \mathbb{R}^{\dim V \times \dim V}$.
(4) Assembly of the matrix $K^{(2)}$.
(5) For all j in V_Γ do
   (a) extraction of the coefficients $K_{mn}^{(2)}, \forall (m,n) \in V_{r,d}^{\{j\}} \times V_{r,d}^{\{j\}}$, and construction of the sparse matrix $\widetilde{K}_{\{j\}}^{(2)} \in \mathbb{R}^{\dim V_{r,d}^{\{j\}} \times \dim V_{r,d}^{\{j\}}}$ with these coefficients;
   (b) computation of the dense matrix $\widetilde{S}_{\{j\}}^{(2)} \in \mathbb{R}^{\dim V_r^{\{j\}} \times \dim V_r^{\{j\}}}$ by condensation of the matrix $\widetilde{K}_{\{j\}}^{(2)}$ on the degree of freedom belonging to $V_r^{\{j\}}$;
   (c) assembly of the matrix $\widetilde{S}_{\{j\}}^{(2)}$ inside the matrix $A_{pp}^{(1)}$.

The matrix $A_{pp}^{(1)}$ could now be used to build the absorbing boundary condition in the sub-domain $\Omega^{(1)}$.

Previously, the case of the approximation of the neighbor Schur complement matrix $K_{pp}^{(2)} - K_{pi}^{(2)}[K_{ii}^{(2)}]^{-1}K_{ip}^{(2)}$ has been described, but all the methodology can be applied for the matrix $K_{pp}^{(1)} - K_{pi}^{(1)}[K_{ii}^{(1)}]^{-1}K_{ip}^{(1)}$ without any particular difficulties. Similar calculation performed in the sub-domain $\Omega^{(1)}$ gives the associated matrix $A_{pp}^{(2)}$.

It is important to notice that for $r = 1$, the sparsity of the matrix $K^{(s)}$ is preserved for any values of d.

In summary, each sub-domain computes for each interface node a local condensation of some degree of freedom belonging to a given set of layers, on a small patch. These local condensations are then assembly and the result is used to build the matrix involved in the absorbing boundary conditions of the neighboring sub-domain.

In fact, this approach is very similar to the finite element methodology. Each patch can be interpreted as a macro-finite element, and the matrix $\widetilde{S}^{(2)}_{\{j\}}$ can be interpreted as an elementary matrix associated to this patch. The matrix $A^{(1)}_{pp}$ is thus similar to the finite element assembly matrix, where all the contribution $\widetilde{S}^{(2)}_{\{j\}}$ are inserted in the matrix $A^{(1)}_{pp}$. The sparse structure of the matrix $A^{(1)}_{pp}$ is issued from the connectivity of the different patch on the interface. Increasing the radius of the patch means increasing the connectivity of the assembly matrix $A^{(1)}_{pp}$. The bandwidth of the local impedance matrix will be larger. As a consequence, each iteration of the iterative algorithm will require additional computations during the forward–backward substitution involved in the solution of the condensed interface problem. For this reason, only small values of the radius have been considered in the numerical experiments.

It is important to mention that in the previous example, $\mathbb{P}_1$-finite elements have been considered for the sake of clarity. When working in linear elasticity, three degree of freedom are associated to each node. As a consequence, the set of degree of freedom associated to the nodes should be considered in place of the set of nodes used in the algorithm.

4.3. General mesh partitioning

In the case of a general mesh partitioning, some cross points may appear, i.e., points where more than two sub-domains intersect. An example of such a configuration is shown in Fig. 4. In this example, the interfaces between the sub-domains $\Omega^{(1)}$ and $\Omega^{(4)}$, or between the sub-domains $\Omega^{(2)}$ and $\Omega^{(3)}$ reduce to a single node. As a consequence, the patch simply reduces to a single node, and the layers are built around this node. It is important to notice that despite the relative complexity to built the patch and the associated layers, the methodology to construct the augmented matrix is the same with or without cross points. Indeed, the notion of the interface is local: each separate interface lies between two sub-domains, and there is no global interface. This implies that the previous description for two sub-domains is easily extended to the general case, and to the case of weak interfaces (corners in 2D, and edges in 3D).

4.4. Block diagonal approximation

An interesting property of the sparse approximation is obtained in the case of a depth d equal to zero. With such a choice, the augmented matrix $A^{(s)}_{pp}$ consists to approximate the neighbor Schur complement matrix $K^{(q)}_{pp} - K^{(q)}_{pi}[K^{(q)}_{ii}]^{-1}K^{(q)}_{ip}$ with its first term, i.e., the stiffness matrix $K^{(q)}_{pp}$, $s, q = 1, 2, s \neq q$ [18,12]. Such an approx-

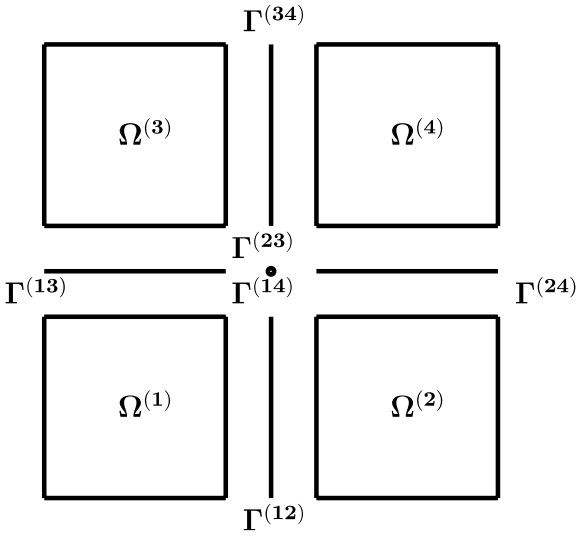

Fig. 4. Example of a domain decomposition into four sub-domains with one cross point.

imation, presents the advantage to be very easy to implement since this matrix is already computed by the sub-domain during the assembly procedure and the integration of the contribution of the interface nodes.

5. Numerical experiments

In this section, an analysis of the proposed technique is presented. A 2D square shaped domain submitted to bending is considered. Homogeneous Dirichlet boundary conditions are imposed on the left side of the domain. Loading, modelled as non-homogeneous Dirichlet boundary conditions are imposed on the right side of the structure. Homogeneous Neumann boundary conditions are set on the top and on the bottom. The domain is meshed with triangular elements and discretized with $\mathbb{P}_1$-finite elements involving two degrees of freedom per node. The mesh is then split into N_s sub-domains. The domain decomposition method with two Lagrange multipliers and two augmented matrices described in this paper is considered. The condensed interface problem is solved iteratively with a Krylov method namely ORTHODIR [23]. The stopping criterion is $\|r_n\|_2 < 10^{-6}\|r_0\|_2$, where r_n and r_0 are the nth and the initial global residuals, and where $\|\cdot\|_2$ denotes the $\mathbb{L}_2$-norm.

Fig. 5 illustrates the initial mesh and the final deformed shape of the domain in the case of a mesh partitioning into four sub-domains.

The asymptotic analysis upon the number of sub-domains is now investigated for a given mesh size equal to $h = 1/400$. The Poisson ratio and the Young modulus are equal to $v = 0.3$ and to $E = 2 \times 10^5$. The domain is split into 4 ($=2 \times 2$), 16 (4×4), and 64 ($=8 \times 8$) sub-domains. It is important to point out the existence of several cross points in the partition, i.e., points where more than two sub-domains intersect. The respective influence of the choice of the augmented matrices on the number of iterations required by the iterative algorithm are reported in Fig. 6. The quality of the augmented matrix can be classified upon the value of the depth used in the sparse approximation. The neighbor Schur complement matrix (which is a dense matrix) gives of course the best results. Since no global preconditioning technique is used increasing the number of sub-domains increases the number of iterations. Later on, using a coarse gird correction as introduced in [7] for acoustic problems will help to achieve a scalability of the domain decomposition method; an issue under current investigation.

The asymptotic analysis upon the mesh size parameter is now investigated for a given mesh partitioning into 64 ($=8 \times 8$) sub-domains. The Poisson ratio and the Young modulus are equal to $v = 0.3$ and to $E = 2 \times 10^5$. The results are reported in Fig. 7. A dependence upon the mesh size can be noticed for all the methods and once again the respective efficiency of the approximations depends of the value of the depth. Choosing the augmented matrix equal to the neighbor Schur complement matrix implies all the degree of freedom of the neighboring sub-domain are condensed on the interface. As a consequence, the number of iteration required by the domain decomposition method is independent of the mesh size.

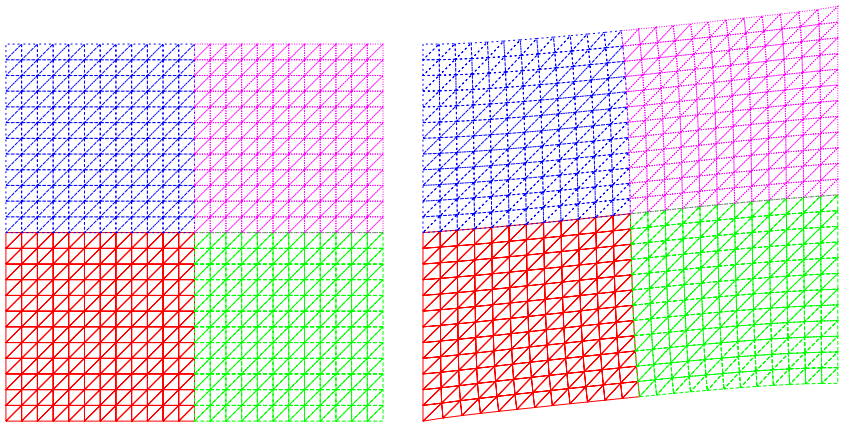

Fig. 5. Initial mesh (on the left) and displacement value (on the right) for the shear problem. Case of a mesh partitioning into 2×2 sub-domains ($h = 1/25$).

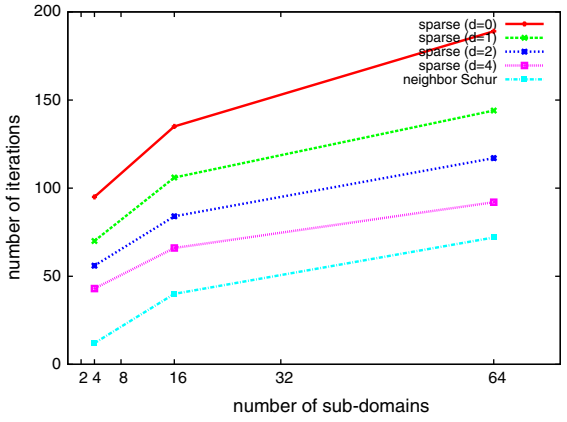

Fig. 6. Asymptotic behavior for different augmented matrices and different number of sub-domains ($h = 1/400$).

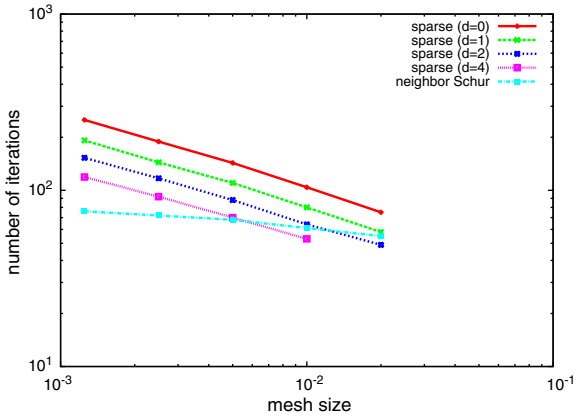

Fig. 7. Asymptotic behavior for different augmented matrices and different mesh size parameter ($N_s = 8 \times 8$).

The asymptotic analysis upon the heterogeneity ratio between the sub-domains is now investigated for a given mesh size $h = 1/400$ and a given partitioning into 3 ($=1 \times 3$) sub-domains. The results reported in Fig. 8 show that increasing the heterogeneity ratio between the sub-domains, reduces the number of iterations! In these experiments the Poisson ratio is equal to $\nu^{(s)} = 0.3$ and the Young modulus $E^{(s)}$ belongs to the range $[2, 2 \times 10^5]$ and it is assumed to be constant per sub-domain. The reduction of the number of iterations can easily be explained. Indeed, the material properties of a given sub-domain are known by the neighboring sub-domains, through the knowledge of the augmented matrix.

The dependence of the method upon both the mesh size parameter and the heterogeneity ratio is now analyzed. A general mesh partitioning into 16 ($=4 \times 4$) sub-domains with several cross points is considered, as represented in Fig. 9. The Poisson ratio and the Young modulus are assumed to be constant per sub-domain and are defined by $\nu^{(s)} = 0.3$ and $E^{(s)} = 2 \times 10^5$ in the sub-domains colored in gray and by $\nu^{(s)} = 0.3$ and $E^{(s)} = 2$ or $E^{(s)} = 2 \times 10^3$ or $E^{(s)} = 2 \times 10^5$ in the sub-domains colored in white. The number of iterations is analyzed upon the augmented matrices considered. The results are reported in Table 1. As expected by the theory, this table clearly shows that increasing the number of layers reduces significantly the number of iterations. Once again, increasing the heterogeneity between the sub-domains reduces the number of iterations. This property is very interesting since increasing the heterogeneity between the sub-domains deteriorates the conditioning number of the global problem, and of the condensed interface problem. Using the proposed augmented matrices, issued from a sparse approximation, gives excellent results. This property is mainly due to the quality of the local DtN map, since this local DtN map models the material property of the neighboring

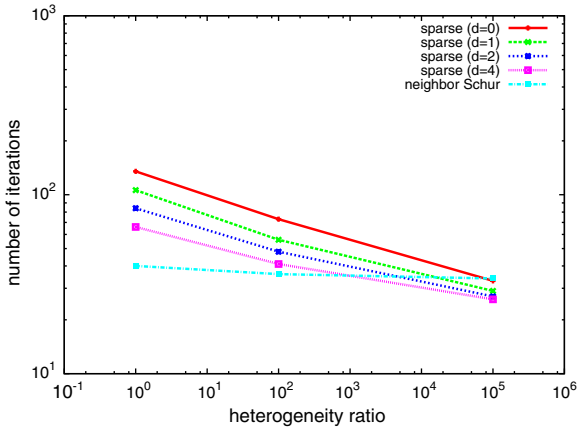

Fig. 8. Asymptotic behavior for different augmented matrices and different heterogeneity ratio between the sub-domains ($h = 1/400$, $N_s = 1 \times 3$).

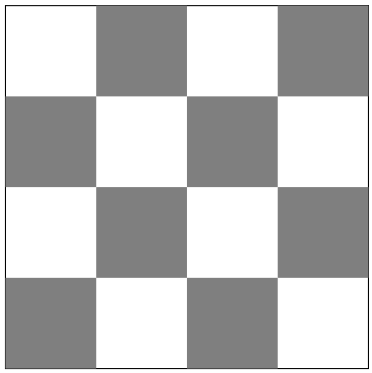

Fig. 9. Domain decomposition into 16 sub-domains.

Table 1
Number of iterations for different augmented matrices, different mesh size parameter and different heterogeneity ratio between the sub-domains ($N_s = 4 \times 4$)

Mesh size	Heterogeneity ratio	Sparse				Neighbor Schur
		($d = 0$)	($d = 1$)	($d = 2$)	($d = 4$)	
1/50	1	54	42	33	–	32
	10^2	34	29	27	26	31
	10^5	29	26	26	25	30
1/100	1	75	59	47	37	35
	10^2	46	36	32	28	34
	10^5	31	27	26	26	31
1/200	1	101	79	63	49	37
	10^2	58	44	39	33	35
	10^5	32	28	27	27	32
1/400	1	135	106	84	66	40
	10^2	73	56	48	41	36
	10^5	33	29	27	26	34

sub-domain. Surprising, the neighbor Schur complement does not always lead to the best convergence. This property is mainly due to the numerical error involved during the computation of the exact Schur complement when dealing with high heterogeneity ratio.

It should be noticed that one iteration of the iterative algorithm requires the same computational time for all the sparse augmented matrices considered, since here $r = 1$. The only difference between the different approximations is located in the preliminary computation of the augmented matrix. Opposite, as already mentioned, the neighbor Schur complement requires much more time during its initial computation and at each iteration of the iterative algorithm. In theory, the neighbor Schur complement corresponds to a sparse approximation with a radius equal to the length of the interface and a depth equal to the width of the sub-domains.

6. Conclusions

The absorbing boundary conditions defined on the interface between the sub-domains are of major importance for the convergence of iterative domain decomposition methods. For linear elasticity problems, optimal absorbing boundary conditions can be determined. These optimal absorbing boundary conditions require the computation of a non-local Dirichlet-to-Neumann map.

In this paper, an original technique to approximate this non-local Dirichlet-to-Neumann map is investigated. This technique is based on the computation of local Dirichlet-to-Neumann maps and is based on the condensation of the degree of freedom belonging to a small area on a small patch. These local Dirichlet-to-Neumann maps are then assembly in order to build a sparse approximation of the non-local Dirichlet-to-Neumann map. The proposed methodology can be assimilated to a finite element method, where each patch is similar to a macro-finite element, and where each local map is similar to an elementary matrix.

Several numerical experiments have been presented for linear elasticity problems with extreme contrasts in the coefficients. The results report impressive and robust convergence of the iterative domain decomposition method equipped with such absorbing boundary conditions. The proposed method offers a good compromise between robustness and efficiency.

References

[1] P. Bjørstad, O. Widlund, To overlap or not to overlap: a note on a domain decomposition method for elliptic problems, SIAM J. Sci. Stat. Comput. 10 (5) (1989) 1053–1061.
[2] C. Farhat, F.-X. Roux, A method of Finite Element Tearing and Interconnecting and its parallel solution algorithm, Int. J. Numer. Meth. Engrg. 32 (1991) 1205–1227.
[3] X.-C. Cai, W.D. Gropp, D.E. Keyes, A comparison of some domain decomposition algorithms for nonsymmetric elliptic problems, in: D.E. Keyes, T.F. Chan, G.A. Meurant, J.S. Scroggs, R.G. Voigt (Eds.), Fifth International Symposium on Domain Decomposition Methods for Partial Differential Equations, SIAM, Philadelphia, PA, 1992, pp. 224–235.
[4] D. Dureisseix, P. Ladevèze, Parallel and multi-level strategies for structural analysis, in: J.-A. Desideri (Ed.), Proceedings of the Second European Conference on Numerical Methods in Engineering, Paris, September 1996—ECCOMAS, Wiley, New York, 1996, pp. 599–604.
[5] C. Farhat, F.-X. Roux, Implicit parallel processing in structural mechanics, in: J.T. Oden (Ed.), Computational Mechanics Advances, vol. 2 (1), North-Holland, Amsterdam, 1994, pp. 1–124.
[6] B. Després, Décomposition de domaine et problème de Helmholtz, C.R. Acad. Sci. Paris 1 (6) (1990) 313–316.
[7] C. Farhat, A. Macedo, M. Lesoinne, F.-X. Roux, F. Magoulès, A. de la Bourdonnaye, Two-level domain decomposition methods with Lagrange multipliers for the fast iterative solution of acoustic scattering problems, Comput. Meth. Appl. Mech. Engrg. 184 (2) (2000) 213–240.
[8] F. Magoulès, K. Meerbergen, J.-P. Coyette, Application of a domain decomposition method with Lagrange multipliers to acoustic problems arising from the automotive industry, J. Comput. Acoust. 8 (3) (2000) 503–521.
[9] F. Collino, S. Ghanemi, P. Joly, Domain decomposition method for harmonic wave propagation: a general presentation, Technical Report No. 3473, INRIA, 1998.
[10] Y. Maday, F. Magoulès, Absorbing interface conditions for domain decomposition methods: a general presentation, Comput. Meth. Appl. Mech. Engrg. in press.
[11] F. Nataf, F. Rogier, E. de Sturler, Optimal interface conditions for domain decomposition methods, Technical Report 301, CMAP (Ecole Polytechnique), 1994.
[12] F. Magoulès, F.-X. Roux, S. Salmon, Optimal discrete transmission conditions for a non-overlapping domain decomposition method for the Helmholtz equation, SIAM J. Sci. Comput. 25 (5) (2004) 1497–1515.

[13] J.D. Benamou, B. Després, A domain decomposition method for the Helmholtz equation and related optimal control problems, J. Comp. Phys. 136 (1997) 68–82.
[14] P. Chevalier. Méthodes Numériques Pour les Tubes Hyperfréquences, Résolution par Décomposition de Domaine, Ph.D. thesis, Université Paris VI, 1998.
[15] M.J. Gander, L. Halpern, F. Nataf, Optimal convergence for overlapping and non-overlapping Schwarz waveform relaxation, in: C.-H. Lai, P. Bjørstad, M. Cross, O. Widlund (Eds.), Eleventh International Conference of Domain Decomposition Methods, ddm.org, 1999.
[16] C. Japhet, F. Nataf, The best interface conditions for domain decomposition methods: absorbing boundary conditions, in: L. Tourrette (Ed.), Artificial Boundary Conditions, with Applications to Computational Fluid Dynamics Problems, Nova Science, in press.
[17] M. Gander, F. Magoulès, F. Nataf, Optimized Schwarz methods without overlap for the Helmholtz equation, SIAM J. Sci. Comput. 24 (1) (2002) 38–60.
[18] F.-X. Roux, F. Magoulès, S. Salmon, L. Series, Optimization of interface operator based on algebraic approach, in: I. Herrera et al. (Eds.), Domain Decomposition Methods in Sciences and Engineering, National Autonomous University of Mexico, Mexico City, Mexico, 2003, pp. 297–304.
[19] F.-X. Roux, F. Magoulès, L. Series, Y. Boubendir, Approximation of optimal interface boundary conditions for two-Lagrange multiplier FETI method, in: R. Kornhuber et al. (Eds.), Domain Decomposition Methods in Science and Engineering, Springer-Verlag, Heidelberg, 2004, pp. 283–290.
[20] P.G. Ciarlet, The Finite Element Method for Elliptic Problems, North-Holland, Amsterdam, 1978.
[21] S. Ghanemi. A domain decomposition method for Helmholtz scattering problems, in: P.E. Bjørstad, M. Espedal, D. Keyes (Eds.), Ninth International Conference on Domain Decomposition Methods, ddm.org, 1997, pp. 105–112.
[22] C. Japhet, F. Nataf, F. Rogier, The optimized order 2 method: application to convection–diffusion problems, Future Gener. Comput. Syst. FUTURE 18 (2001).
[23] Y. Saad, Iterative Methods for Sparse Linear Systems, PWS Publishing Company, 1996.